Numerical modeling and verification of crossed v-groove particle filters

Johan Bejhed, Hugo Nguyen, Peter Åstrand, Anders Eriksson, Johan Köhler

Keywords: Microfluidics, FEM, modeling, filter, massflow, pressure, microsystem, silicon, Poiseuille, Knudsen, Naver-Stokes

Abstract

The gas flow characteristics of a micromachined particle filter has been successfully modelled and simulated. The filter is made by two sets of v-grooves that intersect as two silicon wafers are bonded together. The gas is distributed from inlets via a manifold of channels to the narrow v-grooves.

The fluidic model is derived from the Navier-Stokes equations and assumes laminar isothermal flow and incorporates Knudsen corrections and Poiseuille number calculations. The simulations use the finite element method.

Several elements of the full filter model is treated separately before lumping them together: the straight v-grooves, a single crossing in an infinite set, and a set of exactly four crossings along the flow path. The introduction of a crossing effectively corresponds to a virtual reduction of the length of the flow path, thereby defining a new effective length. The first and last crossings of each flow path together contribute to a pressure drop equal to that from three ordinary crossings.

The derived full filter model has been compared to previous experimental results on several different crossed v-groove filters. Within the experimental errors, the model corresponds to the mass flow and pressure drop measurements. The main error source is the uncertainty in v-groove width which has a profound impact on the fluidic behaviour.

Introduction

In many MEMS applications involving streaming gas, the need of particle free gas is prominent. The delicate MEMS structures are in many applications very sensitive to particles. With filters incorporated within the MEMS module, handling and assembly will be significantly simplified, since particle free integration environment becomes less critical. Micro propulsion for spacecrafts, realized using MEMS technology, is one of many areas where guaranteed particle free gas is required. In space applications, an incorporated filter serves an additional purpose. A standalone filter needs additional housing and leakage tight connections, which both require extensive testing and verification. The additional cost for this is omitted when the filter stack is integrated directly in the MEMS-module

The filter modeled in this paper basically consists of two sets of narrow v-grooves etched into the eventually bonded surfaces of two silicon wafers. The v-grooves form a crossing of 90°angle in-between the two wafers. In addition, each wafer contains its own, much larger, gas-distributing channels. Both wafers are also equipped with through-wafer vias, serving as either gas inlets or outlets, depending on gas flow direction.

Microfluidics is a vast and important field since the advent of microsystems, and has been the topic of several reviews [1-6], focusing on different aspects. In particular, the seminal review

by Gravesen et al [2] is the first to incorporate relevant fluid mechanics, and also points to the increasing use of numerical modelling, and highlights the frequent breakdown in microscale of conventional assumptions. The relevance of microfluidics analysis and modelling was not truly recognized before microstructures became readily available. Fundamental work was done e.g. by Harley and co-authors [7-8]. A recent generalized approach to numerical modelling in microfluidics is presented by Chatterjee [9], which naturally includes the finite element method based on the Navier-Stokes formulas that we use in this paper. The use of these formulas in microdevices simulations was detailed by Jie et al. [10], and numerical modelling of gas flow in microchannels was specifically studied by Jain and Lin [11]

Microfluidic filters have been researched for many applications, e.g. blood plasma separation [12], screening of particles [13, 14], gas separation [15], cleaning of drug infusions [16], and blood or yeast filtration [17, 18]. Commonly, perforated membrane architectures are employed, for example by the group in Twente [17]. This differs distinctly from the design in this paper, where the filter utilizes flow in long, micrometer-wide channels.

From a design point of view, this filter is related to the drug-cleaning filter [16] – that uses a set of v-grooves narrower than 24 µm to perform filtration – and the blood plasma separation filter [12] – where a barrier's height between two large v-groove liquid distributing channels performs the separation. Both of these filters are located at the bond interface of two wafers.

The conceptual design of the crossed v-groove filter was first presented in [19], but has not been thoroughly modeled before. The modeling is validated using experimental data from another paper by the authors [20].

Micromachined crossed v-groove filter summary

A robust and straightforwardly integrated particle filter for gas handling microsystems was manufactured and characterized in a previous study [20]. The filter is formed by crossing narrow v-grooves etched in the surfaces of two wafers that are subsequently bonded. The gas is distributed via larger channels to the intersecting v-grooves. The major points of that study are briefly summarized in the following.

The geometrical accuracy of the narrow v-grooves strongly affects the fluidic performance of the filter, and has been thoroughly determined. The mass flow as a function of inlet pressure has been determined for crossed v-groove filters with nominal width 1.5 µm and 2.0 µm, and also for sets of straight v-grooves, 1.5 µm, 2.0 µm, 3.0 µm, and 4.5 µm, nominally.

The pressure-dependent mass flow through these crossed v-groove filters was preliminary described by introducing a proportionality constant C according to the simple model

$$p_{In}^2 - p_{Out}^2 = C\dot{m}\frac{LS^2}{A^3 N} \qquad \textbf{Eq. 1}$$

For this equation to be valid, the temperature must be constant (at 300 K), and the flow is assumed to be laminar.

Through linear fit of experimental data, the constant C was found to be 1.7 ±0.1 N^2 s/kg m for a 1.5 µm crossing v-groove filter, and correspondingly 2.1 ±0.2 N^2 s/kg m for a 2 µm crossing v-groove filter. Through these experimental values the mass flow through differently designed v-groove filters can be estimated, provided that these designs do not differ too much from the evaluated samples.

The flow rate dependence of width and length of the v-groove are in good agreement with the simplified theory; however, disagreement between crossing v-groove filters and straight v-groove filters remains, and may depend on non-ideal flow conditions.

There is thus a clear identified need thorough numerical modeling of the filter, in order to describe the effects of *e.g.* flow rarefaction (Knudsen corrections), slip flow conditions, velocity-field perturbations, and Poiseuille number derivations. This may allow us to derive a model that can accurately predict the flow performance of any crossed v-groove filter, without the need of additional experiments in order to derive a useful constant C. For the simplified model ([20], and above), this is not the case, as this requires experimental base data from a similar device in order to yield fair predictions on other designs.

Modeling

Before a full filter model can be achieved, some initial modeling must be performed. First straight channels must be modeled. In addition, any effects in the crossings must be investigated. Finally, the filter boundaries, *i.e.* the first and last crossing must be properly modeled.

General assumptions must be made regarding the flow through the filter. The flow through the filter or channels is assumed to be laminar and isothermal (*i.e.* constant temperature). Any compressible effects are ignored, *i.e.* the density of the gas may vary, but any temperature changes due to expansion/compression are not considered, and effects of rarefied gas are taken into account when straight channel flow is modeled, but omitted in filter crossing modeling. With these elements in place, a full filter model can be assembled.

Sample description

There are two different types of filters evaluated. The first group only contains many parallel narrow v-grooves, starting and ending in the distribution channels. The v-grooves are only present in one wafer.

The second group has many parallel v-grooves in both wafers. When bonded together these v-grooves will form crossings. The quite extended crossing region is centered between the distribution channels, but the v-grooves in both wafers do not meet the distribution channels in both wafers. There are a small length, “dead path”, leading the gas into, and out from, the crossing region.

The geometrical properties where thoroughly evaluated in [20], and here only presented in a summarized form Table 1, for completeness.

Table 1 Characteristics of evaluated samples, all lengths in µm

ID	Type	Nominal Width	Resulting Width	95% Conf.	Nominal Length	Resulting Length	Number of Channels
1	Filter	2.0	2.5	±0.2	35.1	31.5	49500
2	Straight	2.0	2.5	±0.2	7.0	3.4	150000
3	Filter	2.0	2.5	±0.2	62.6	59.0	50400
4	Filter	1.5	1.9	±0.2	28.4	24.8	84882
5	Filter	1.5	1.9	±0.2	54.6	51.0	84440
6	Filter	1.5	1.9	±0.2	79.4	75.8	84740
7	Straight	2.0	2.5	±0.2	80.0	76.4	160000
8	Filter	2.0	2.5	±0.2	90.5	86.9	49980
9	Straight	3.0	3.3	±0.2	40.0	36.4	5000
10	Straight	4.5	4.9	±0.2	40.0	36.4	1600

Straight channels

The theory of straight channels is based on the ideal gas law, and the steady state formulations of the mass conservation equation and Navier-Stokes equation. These equations are summarized in eq 1-3:

$$p = \rho RT \qquad \textbf{Eq. 2}$$

$$\nabla \cdot (\rho u) = 0 \qquad \textbf{Eq. 3}$$

$$\rho(u \cdot \nabla)u = -\nabla p + \mu \nabla^2 u \qquad \textbf{Eq. 4}$$

where p is the pressure, ρ the gas density, R_m the gas constant (adjusted to N_2), T the temperature, μ the viscosity, and u the gas velocity.

The flow development length is commonly defined as the length required until the maximum flow velocity has reached 99% of the fully developed flow, and can be calculated using the hydraulic diameter (D_h) and Reynolds number (Re), according to [2].

$$D_h = \frac{4 \cdot Area}{Perifery} \qquad \textbf{Eq. 5}$$

$$\mathrm{Re} = \frac{\rho \bar{u} D_h}{\mu} \qquad \textbf{Eq. 6}$$

$$L_d = 0.03 D_h \mathrm{Re} \qquad \textbf{Eq. 7}$$

Considering that the Reynolds number are small (Re≈100) and given the very small dimensions in MEMS fabricated filters, the development length will be very short (around 0.4 μm).

From the ideal gas law and the steady state formulations of Navier-Stokes equations, combined with mass conversion and an assumed short flow profile development length, the squared pressure drop over a channel of length L becomes

$$(p_{in})^2 - (p_{out})^2 = \frac{4LPo\mu RT}{D_h^2 A}\dot{m} \qquad \textbf{Eq. 8}$$

where $\dot{m}$ is the mass flow thought the channel. p_{in} and p_{out} are the inlet and outlet pressures. The channel geometry is described by its area, (A), hydraulic diameter, (D_h) and Poiseuille number (Po).

The Poiseuilles number (Po) for a regular triangle is found in the literature [21]. The cross section of a fully etched v-groove in a silicon wafer is not a perfect regular triangle. The (111) direction in silicon crystal forms a 54.7°angle with the (100) plane. Thus, two angles of the cross sectional triangle will be 54.7°. Poiseuilles number for this triangle is calculated numerically, using the computer software "Comsol Multiphysics", developed by Comsol [22]. Poiseuilles number can be calculated using the expression [21,23]

$$Po = C_f \mathrm{Re}_{Dh} = C_f \frac{\rho \bar{u} D_h}{\mu} \qquad \textbf{Eq. 9}$$

where C_f is the Fanning friction factor, defined as $C_f = \frac{2\tau_w}{\rho \bar{u}^2}$. The shear ($\boldsymbol{\tau}$) and velocity are achieved by the means of FEM studies, giving information of the Poiseuilles number.

In addition to these fundamental flow equations, rarefaction effects are taken into account by using the Knudsen number when setting the boundary conditions. The Knudsen number is defined as the ratio between the mean free path of the gas and a characteristic length in the

system. $Kn = \frac{\lambda}{D_h}$ where D_h is choosen as the characteristic length. The rarefaction effects in the flow are taken into account in the flow equations by replacing the non-slip boundary conditions at walls by the Knudsen-corrected boundary condition

$$u_w = \lambda \frac{du}{dz} = l_{char} Kn \frac{du}{dz} = l_{char} Kn(n \cdot \nabla u) \quad \textbf{Eq. 10}$$

Combining the expressions of mean free path and ideal gas low, the Knudsen number becomes inversely proportional to the pressure. Thus, corrections due to non-zero Knudsen number can be added to the pressure drop equation for a straight channel which then becomes

$$(p_{in} + kKn_0 p_0)^2 - (p_{out} + kKn_0 p_0)^2 = \frac{4LPo_0 \mu RT}{D_h^2 A} \dot{m}, \quad \textbf{Eq. 11}$$

where Kn_0 is Knudsen number at p_0, whilst Po_0 is the Poiseuille number at Kn=0. k is dimensionless and represents the Knudsen-number corrections for the flow.

Single crossing

The filter comprises large numbers of straight v-grooves, thus the relations derived earlier can only be used for the straight-channels part of the filter, or for the filters that only comprise straight v-grooves. Differences arise when crossings are introduced. 3-D FEM studies were performed to investigate the flow behavior through a crossing. It is highly inefficient and inconvenient to study the entire set of crossings, why only one crossing was initially investigated, and later this was expanded to a set of four crossings.

A v-groove filter is basically two perpendicular v-grooves. In the crossing region the channels cross sectional area are significantly increased, and the gas also has the possibility to change direction, *i.e.* change v-groove.

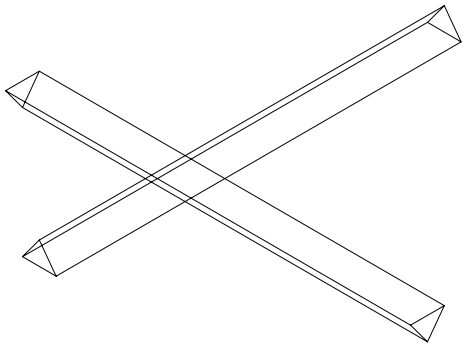

Figure 1 A single crossing studied with FEM

Over the line of one v-groove many perpendicular v-grooves crossings are found. The velocity profile after one v-groove will be the incoming velocity profile to the next crossing, and yet again the output velocity profile from the second crossing will be the incoming velocity profile to the third crossing, and so on. This symmetrical design allows for the use of periodic boundary conditions.

However, the use of periodic boundary conditions depends strongly of the velocity profile, *i.e.* the flow must be fully developed before entering the following crossing in order to be convenient formulated. Thus, the behavior immediately after a crossing must be investigated in order to validate this assumption. If the flow profile is not fully developed before the next v-groove crossing, the periodic boundary condition cannot be used. Also, the periodic

boundary conditions assume an infinite number of crossings, which clearly is not the case. This could also limit the eventual applicability of the model.

From Eq. 7, the development length at Reynolds number around 100 is found to be about 0.4μm, thus the flow profile will, theoretically, be fully developed before entering the next crossing.

Boundary effects at the edges of the filter

The number of crossings for a single v-groove is limited. Special investigations regarding the first and last crossing must be performed, since these points differ from the centrally positioned crossings. The first and last crossings have only two free gas flow paths, compared to three for the other. To investigate the boundary behavior, an increased model was used. This model contains a total of four crossings, where the middle two are identical to the single crossing model, but the first and last crossing has only three possible gas channels. With this increased model the boundary effects can be established, and also the validity of the single channel crossing model can be verified. If the four-crossing model deviates severely from the single crossing model, earlier assumptions are flawed. Figure 2 is a schematic illustration of the four crossing model.

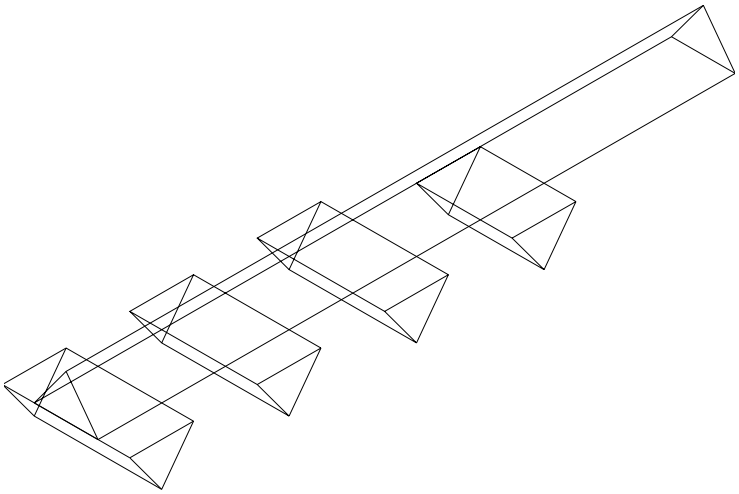

Figure 2 Increased mode to investigate the flow behavior through several. Note the right most crossing and the left most crossing only has three channels intersecting each.

Lumped full filter model

Once the one-crossing model is successfully derived, the whole filter can rather easily be modeled. A segment of a filter contains a straight channel, *i.e.* the dead path, and a crossing. The difference from any arbitrary chosen crossing segment and the following segment is merely the inlet pressure, *i.e.* the pressure drop, and the density.

The pressure drop over one segment is the combined pressure drops over the straight channel and the crossing, and can be expressed as $p_N^2 - p_{N-1}^2 = f_N + g_N$, where f and g are the quadratic pressure drop functions for the channel and the crossing respectively. Index N indicates any arbitrary crossing. The total pressure drop over the filter can then be expressed as the sum of all individual pressure drops, as $p_{In}^2 - p_{Out}^2 = \sum_{n=1}^{N} (f_n + g_n)$. The squared pressure drop over the crossing region is shown in Eq. 12 and the pressure drop over the dead path is shown in Eq. 13

$$\left(p_{in}+kKn_0p_0\right)^2-\left(p_{out}+kKn_0p_0\right)^2=\frac{2L_0Po_0\mu RT}{D_h^2AM}\dot{m} \qquad \textbf{Eq. 12}$$

$$\left(p_{in}+kKn_0p_0\right)^2-\left(p_{out}+kKn_0p_0\right)^2=\frac{4L_{dp}Po_0\mu RT}{D_h^2AM}\dot{m} \qquad \textbf{Eq. 13}$$

where L_0 corresponds to the designed length of the crossing region, and L_{dp} is the dead path to the crossig region.

Results

Straight channels

Solving Eq. 9 numerically for the triangular geometry gives the Poiseuille number Po=13. This value diverges very little from values found in the literature for a regular triangle, *i.e.* 13.33. [21]

By setting the Knudsen number to zero, the Poiseuille number at Kn=0 could be calculated. By increasing the Knudsen number, and subsequently re-calculating the Poiseuille number, a linear curve was obtained, as shown in Figure 3. Thus Poiseuille number can be expressed as a linear function of the Knudsen number, according to $Po = Po_0/(kKn_0+1)$, where Po_0 is Poiseuille number at Kn=0. The slope 8k) of the generated line was found to be k=8.

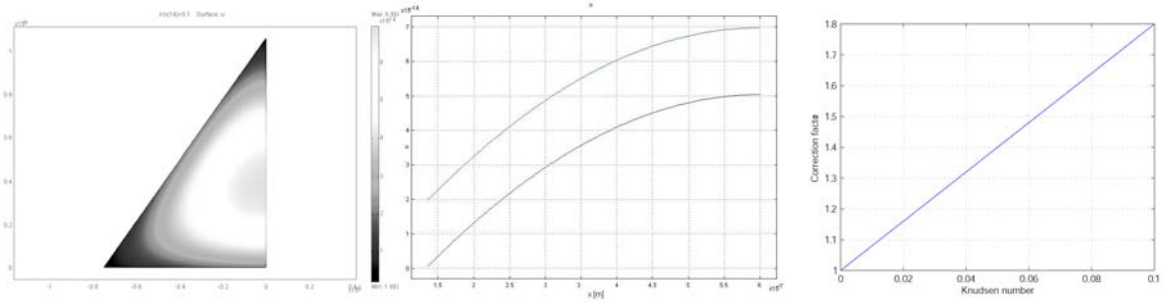

Figure 3 A) Velocity profile for one v-groove, and the corresponding velocity profiles for 2 different Knudsen values (B). Repeating the process for several Knudsen numbers gives a linear plot, shown in C, where k=8.

Single crossing

From the single crossing model, the pressure drop along a channel is obtained, shown in Figure 4. The crossing is clearly shown in the center of the graph as a region with less pressure drop rate. The model indicates that the crossings can be treated as straight channels, if an offset in the pressure drop between the inlet and outlet are introduced. This offset can be represented as a new effective length (L_{eff}) according to $L_{eff}=(L_0-0.874D_h)$. Since each v-groove crosses another v-groove N times, the effective length will be reduced to $L_{eff}=\left(L_0-0.874D_hN\right)$.

This reduction of length is valid if the gas density variation in the crossing is negligible, and the numerical value is only valid for V-shaped channels, crossing at 90° angle. However, the value is valid for any type of gas and flow velocities, as long as the Reynolds number is low enough, and any Knudsen number corrections can be ignored.

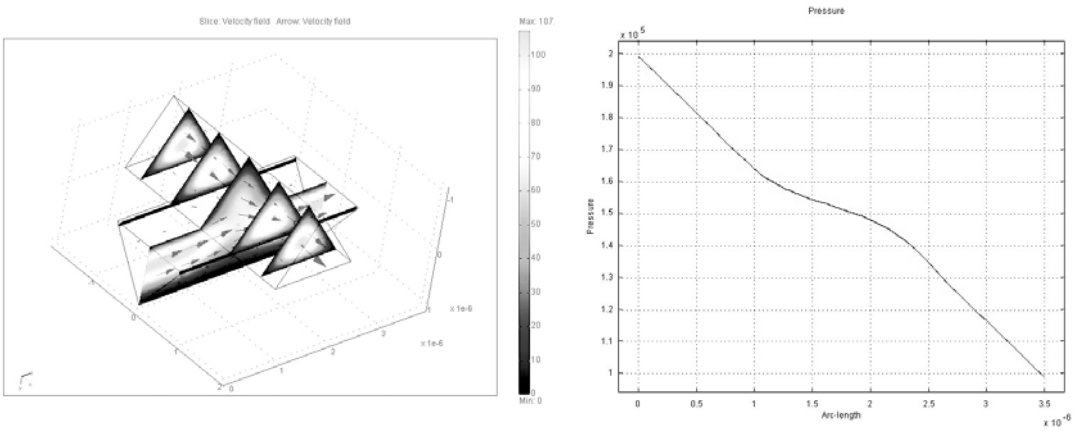

Figure 4 Left: The simulated pressure drop in a crossing. Right: The pressure along the length of the crossing. Note the planar region corresponding to the crossing.

Four crossing model

The result from the four crossing model is very important. First, the two center crossings in Figure 5 behave very similar to the simulated single crossing. Thus, the assumption of an infinite number of crossings is valid for as few as four crossings. Also, boundary effects between two adjacent crossings are clearly insignificant, as expected from the very short development length. This implies that simple crossings simulations hold ground in aspects both of assumed boundary condition, as well as the low impact of other crossings from the single-crossing behavior.

However, the first and last crossings have slightly different behavior as compared to the ones in between. The pressure drop over these two crossings represents 1.5 times an ordinary crossing each. Thus, the first and last crossing will together behave as three crossings. A filter design with N crossings must then be treated as a filter with N+1 crossings, due to this first and last boundary effect.

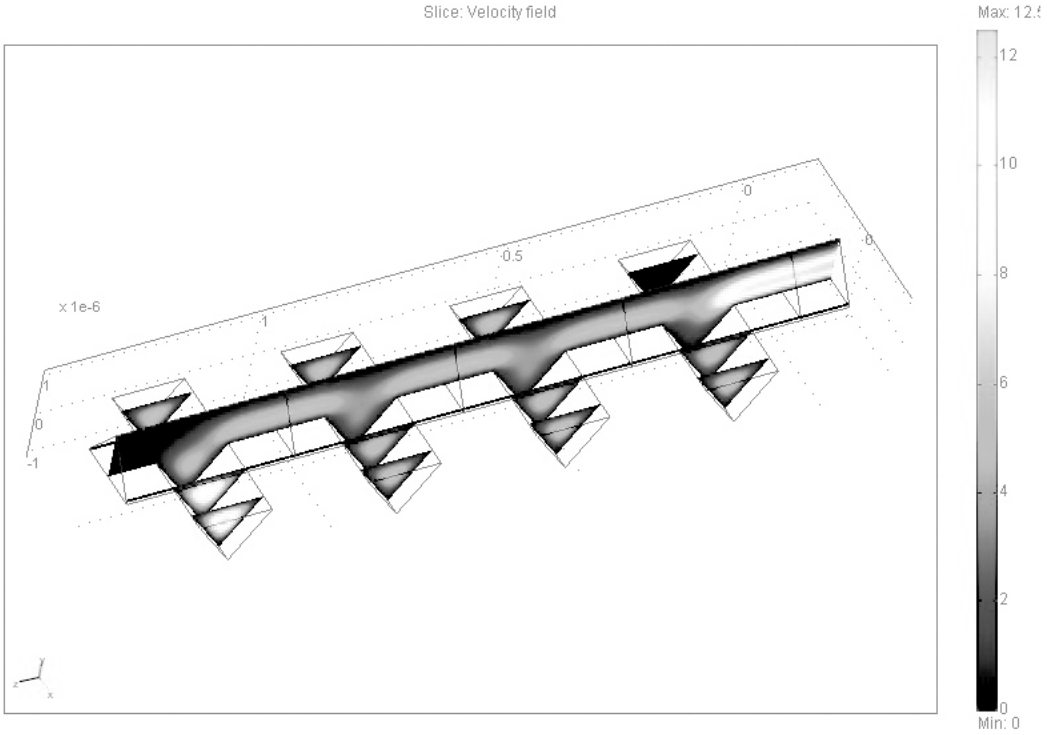

Figure 5 Simulated behaviour for a set of four crossings. Note the deviation of stream possibilities for the first and last crossing. Also, the two center crossings behave similar.

Summary of modeling

The Poiseuilles number was numerically found to be 13.33, which deviates very little from values found in the literature. Furthermore, the linear term k, describing the Knudsen number for different Poiseuilles numbers was found to be 8.

The single crossing simulation indicates that a v-groove crossing can be modeled as a small shortening of the actual v-groove length. A v-groove, crossed N times, will have an effective length of $L_{eff} = \left(L_0 - 0.874 D_h N\right)$.

Boundary conditions, in terms of first and last crossing in the v-groove filter, shows slightely different behavior compared to the central positioned crossings. The pressure drop per crossing is 1.5 times a central positioned. Thus, a filter with N crossings must be modeled as a filter with (N+1) crossings, resulting in a new effective length according to

$$L_{eff} = \left(L_0 - 0.874 D_h (N+1)\right). \qquad \textbf{Eq. 14}$$

Also, in the crossing region there are equal amounts (M) of v-grooves in both wafers, giving 2M parallel throughout the crossing region.

The straight filter and the dead path leading in and out of the crossing v-groove region can be modeled in series [24] according to

$$\left(p_{in} + kKn_0 p_0\right)^2 - \left(p_{out} + kKn_0 p_0\right)^2 = \frac{4 L_S Po_0 \mu RT}{D_h^2 AM} \dot{m} \qquad \textbf{Eq. 15}$$

whilst the crossing region follows

$$\left(p_{in} + kKn_0 p_0\right)^2 - \left(p_{out} + kKn_0 p_0\right)^2 = \frac{2 L_{eff} Po_0 \mu RT}{D_h^2 AM} \dot{m} \qquad \textbf{Eq. 16}$$

where k=8 and Po_0=13.33. In Eq. 15 L_s denotes either the length of the dead path or the length of the straight filter.

Discussion

The dependence of the actual v-groove width is strongly represented in for instance Eq. 15, (inversely proportional to w^4). Simulations were performed for the three different values of the v-groove width. The nominal value represents the average v-groove width, and the additional values forms the 95% confidence interval, based on the assessment of width variance [20]. The geometrical properties of the samples are listed in Table 1

Also, the samples evaluated exhibit deviating behavior at higher pressures, possible originating from internal leakage within the sample [20]. Due to this, theory versus measurement comparisons were only performed at lower pressures ($p \leq 2.5$ bar). Also, at higher pressures the Mach numbers increases significantly, which conflict with the boundary conditions in the theory.

The large quantity of noise, especially at low pressures, is due to the measurement equipment. Thus, the use of measured values at mass flows approaching zero, *i.e.* small pressure drops must also be avoided.

Figure 6 shows sample 1 and 4 and are representative examples of the measurements. Sample 1 shows reasonable agreement with theory at low Mach-numbers, *i.e.* $p \leq 2.5$ bar pressure. Sample 4 shows excellent agreement for a wider flow range. As a precaution, only low pressures were used when calculating the ratio between theory and experiments.

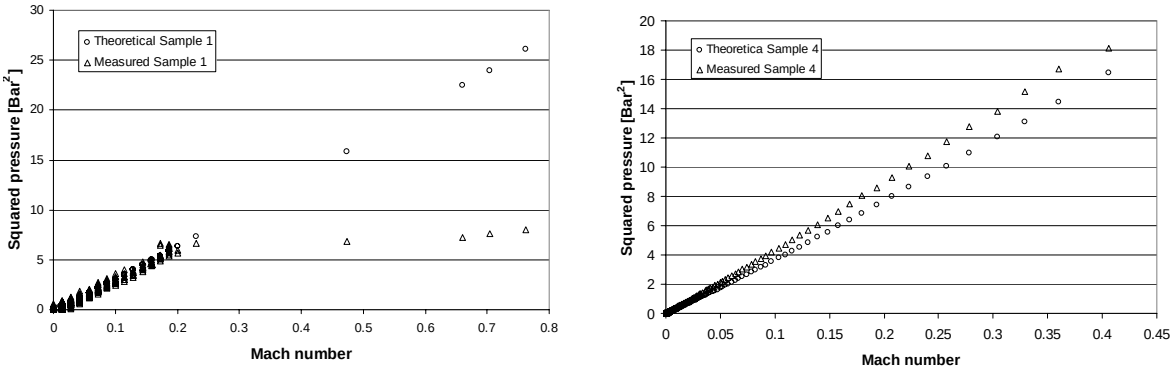

Figure 6 Modelled and measured flow through a filter for the samples 1 and 4. Note the strong deviation above Mach-number 0.2 for sample 1.

The same results are shown again in Figure 7, but now as the ratio between theory and experiments. The data set shown in Figure 7 is for the average v-groove width. Similar charts for the upper and lower 95% confidence interval was also generated, but not shown here. Instead this calculation procedure is repeated for all samples, three v-groove widths per sample. The achieved ratios are presented graphically in Figure 8 (averaged values for low flows).

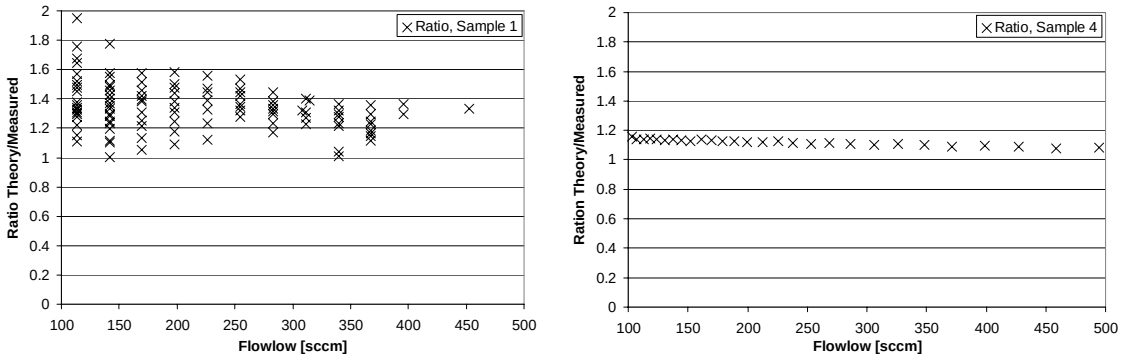

Figure 7 Ratio between modeled and experimental values for sample 1 and 4, at nominal v-groove width. The appearance of sample 1 is due to noise in the measurement equipment.

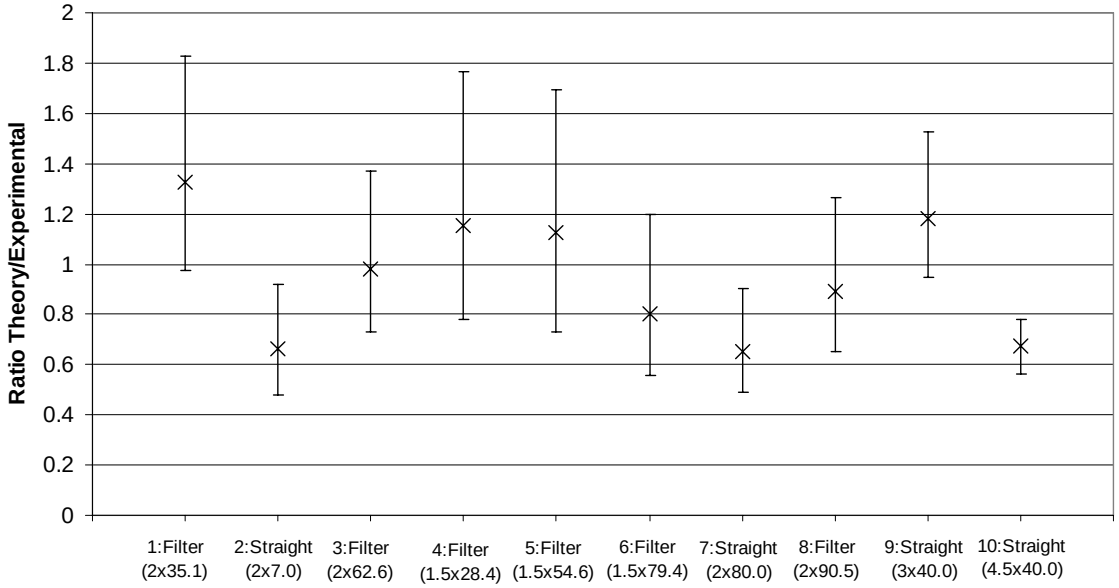

Figure 8 Visualization of the model correspondence to experimental results for all samples. Information given in the label is the sample number, type, v-groove width x v-groove length (units in µm).

The uncertainty in v-groove width determination has a strong effect on the overall accuracy of the simulation compared to the experiments. This is the cause of the rather wide confidence intervals. Note, for instance, that samples 4 and 5 are both nominally 1.5 μm wide, whilst sample 10 is 4.5 μm wide, and the difference of their respective confidence intervals is clearly very large. Thus, the uncertainty becomes less important if the nominal v-groove width increases, as is apparent in the diagram.

Sample 1, 7, and 10 are the only three samples that do not overlap ratio 1.0. They all lack v-groove crossings. Despite the slightly low ratio, all the samples correspond perfectly with respect to each other.

Most samples in Figure 8 originate from measurements on crossed v-groove filter and they all overlap ratio 1.0. Also, the nominal values are close to one. This means that the model derived and used in this paper to describe the flow is significantly improved compared to the initial simple approach used previously [20].

Not included in this data treatment is the effect of the different shortening of the channels, due from the formation of the distribution channels. However, the length is only linearly represented in Eq. 15 and Eq. 16, whilst the width is represented as the power of four. The variation in lengths will have some minute effect on samples with very short v-groove length, like sample 2. The effect on the other samples is negligible.

With the results from the modeling, predictions of the flow through a crossed v-groove filter can be achieved with good accuracy, without the need of further experimental validation or prior measurements on similar filters.

Conclusions

The extended theoretical approach, including FEM simulations of single and multiple v-groove crossings, derived and verified in this paper enables the prediction of the flow behavior of a crossed v-groove filter. The model shows good agreement with experimental values from previous measurements.

The model represents the squared pressure drop over the filter as a function of the mass flow. This function is a summation of two separate expressions, one for the straight v-groove part, and one for the crossing region. For the crossing region, the effect of each crossing is modeled as a reduction of the v-groove length. Moreover, the first and last crossing together make an impact equal to three ordinary crossings, from being the boundary of the crossing region.

However, straight channels are not perfectly predicted with this extended approach. The straight channels agree well within their group, but the theory underestimates the pressure drop as a function of mass flow, even given the 95% confidence interval. Despite that, the confidence interval of the crossing filter and the straight filter do overlap, to some extent.

Acknowledgement

European Space Agency (ESA) is acknowledged for funding this project through the contracts 18829, 18592, and 11041.

References

1. van de Pol, F. C. M. And J. Branebjerg, Micro Fluid-Handling Systems – state of the art and opportunities, 5th Int. Conf. Advanced Robotics, 19-22 June, Pisa, Italy, pp 283-290, 1991.
2. Gravesen, P., J. Branebjerg, and O Søndergård Jensen, Microfluidics – a review, Journal of Micromechanics and Microengineering, **3**, pp 168-182, 1993.
3. Shoji, S. and M. Esashi, Microflow devices and systems, Journal of Micromechanics and Microengineering, **4**, pp157-171, 1994.
4. Stemme, G. Micro Fluid Sensors and Actuators, 6th Int. Symp. Micro Machine and Human Science, 4-6 Oct, Nagoya, Japan, pp 45-52, 1995.
5. Zengerle, R. and H. Sandmaier, Microfluidics, 7th Int. Symp. Micro Machine and Human Science, 2-4 Oct, Nagoya, Japan, pp 13-20, 1996.
6. Verpoorte, E. and N. F. de Rooij, Microfluidics meets MEMS, Proc. IEEE, 91 (6), 930-953, 2003.
7. Harley, J. C., Compressible gas flows in microchannels and microjets, PhD thesis, University of Pennsylvania, 1993.
8. Harley, J.C., Huang, Y., Bau, H. H., and Zemel, J. M., Gas flow in micro-channels, Journal of Fluid Mechanics, 284, pp 257-274, 1995.
9. Chatterjee, A., Generalized numerical formulations for multi-physics microfluidics-type applications, Journal of Micromechanics and Microengineering, **13**, pp 758-767, 2003.
10. Jie, D., X. Diao, K. B. Cheong, and L. K. Yong, Navier-Stokes simulations of gas flow in micro devices, Journal of Micromechanics and Microengineering, 10, pp. 372-379, 2000.
11. Jain, V., and C. X. Lin, Numerical modeling of three-dimensional compressible gas flow in microchannels, Journal of Micromechanics and Microengineering, 16, 292-302, 2006.
12. Brody, J. P., T. D. Osborn, F. K. Forster, P. Yager, A planar microfabricated fluid filter, Sensors and Actuators A, **54**, pp 704-708, 1996.
13. Stemme, G., and G. Kittilsland, New fluid filter structure in silicon fabricated using a self-aligning technique, Applied Physics letters, **53** (16), pp 1566-1568, 1988.
14. Kittilsland, G. and G Stemme, A Sub-micron Particle Filter in Silicon, Sensors and Actuators A, **21-23**, pp 904-907, 1990.
15. Tong, H. D., F. C. Gielens, J. G. E. Gardeniers, H. V. Jansen, J. W. Berenschot, M. J. De Boer, J. H. De Boer, C. J. M. Van Rijn, and M. Elwenspoek, Microsieve supporting palladium-silver alloy membrane and application to hydrogen separation, Journal of Microelectromechanical Systems, **14** (1), pp 113-124, 2005.
16. Drake, J. and H. Jerman, A precision flow restrictor for medical infusion therapy, 8th Int. Conf. Solid **State** Sensors and Actuators, and Eurosensors IX, June 25-29, Stockholm, Sweden, pp. 373-376, 1995.

17. Kuiper, S., C. J. M. van Rijn, W. Nijdam, and M. C. Elwenspoek, Development and application of very high flux microfiltration membranes, Journal of Membrane Science, **150**, pp 1-8, 1998.

18. van Rijn, C. J. M. and M. C. Elwenspoek, Micro filtration membrane sieve with silicon micro machining for ibdustrial and biomedical Applications, Proc. IEEE Micro Electro Mechanical Systems, 29 Jan-2 Feb, pp 83-87, 1995.

19. Köhler, J., J. Bejhed, H. Kratz, U. Lindberg, K. Hjort, and L. Stenmark, A hybrid cold gas microthruster system for spacecraft, Sensors & Actuators A, **97-98** 587-598, 2002.

20. Bejhed, J., H. Nguyen, A. B. Eriksson, L. Stenmark, J. Köhler, Characterization of a particle filter made from crossed v-grooves in silicon, submitted to Journal of Micromechanics and Microengineering, 2006.

21 White, F. M., Poiseuille flow through ducts, in Viscous fluid flow, 2nd ed., ISBN 0-07-069712-4, McGraw-Hill Series in Mechanical Engineering, New York, pp 114-132, 1991.

22 Comsol Multiphysics, www.comsol.com, May 2006.

23 Poiseuille's number: Park, S-J., S. Chung, H-W. Bang, C. Chung, D-C. Han, and J-**K** Chang, Modeling and designing of microfluidic system using Poiseuille number, 2nd Ann. Int. IEEE-EMBS Spec. Topic Conf. Microtechnologies in Medicine & Biology, May 2-4, Madison, Wisconsin, pp 565-568, 2002.

24 Cheng, K. B., M. Wong, and Y. Zohar, Parallel and series multiple microchannel systems, Proc. IEEE 16th Ann. Int. Conf. Micro Electro Mechanical Systems, 19-23 Jan, Kyoto, Japan, pp. 291-294, 2003.